Vol 13 No 9, September 2004
1009-1963/2004/13(09)/1537-07

Chinese Physics

© 2004 Chin. Phys. Soc.
and IOP Publishing Ltd

Electron transport across a quantum wire embedding a saw-tooth superlattice*

Chen Yuan-Ping(陈元平)‡, Yan Xiao-Hong(颜晓红)†,
Lu Mao-Wang(卢卯旺), and Deng Yu-Xiang(邓宇翔)

Institute of Modern Physics and Department of Physics, Xiangtan University, Xiangtan 411105, *China*

(Received 17 November 2003; revised manuscript received 27 April 2004)

By developing the recursive Green function method, the transport properties through a quantum wire embedding a finite-length saw-tooth superlattice are studied in the presence of magnetic field. The effects of magnetic modulation and the geometric structures of the superlattice on transmission coefficient are discussed. It is shown that resonant peak splitting of this kind of structure is different from that of 'magnetic' and 'electric' superlattices in two-dimensional electron gas. The transmission spectrum can be tailored to match requirements through adjusting the size of saw-tooth quantum dot and field strength.

Keywords: finite-length superlattice, saw-tooth quantum dot
PACC: 7320D, 7340G

1. Introduction

With the development of microfabrication techniques, it is possible to construct various kinds of low-dimensional semiconductor structures, such as superlattices, quantum wires, and quantum dots. This spurs wide investigations of electron transport in complex quantum potential structures.[1−9] For instance, contrary to the quantized conductance in units of $2e^2/h$ for a perfect quantum wire, abrupt change of geometry in quantum wire may destruct the simple step-like form and thus produce rich quantum phenomena and have many applications. So various aspects of non-uniform quantum wires or waveguides, such as quantum interference in T-Stub waveguide,[1] bound states in bent quantum wire,[2] resonant tunnelling in double constriction,[3] etc, have been studied in detail. For the electron transport properties of these quantum wires, magnetic modulations as well as the structure of potential barriers are found to be important factors. It is found that the presence of magnetic modulation may cause a variety of new quantum phenomena.[4,5] Recently, a kind of complex quantum structures was presented to describe electronic transmission under periodic potential modulations and/or magnetic modulation.[6−9] If the one-dimensional quantum channel is modulated by a periodic potential or patterned with a periodic structure, minigaps of zero density of state and minibands are expected to form. The formation of minibands and minigaps in a finite lateral superlattice has been produced using a split-gate technique, in which the one-dimensional lateral surface superlattice is realized by a periodic modulation of constriction width.[6] Xu[7] and Gu *et al*[8] investigated the electronic transport through a quantum wire or waveguide embedding a finite one-dimensional electric superlattice. It is found that conductance quantization is recovered under magnetic modulation. Ji and Sprung[9] calculated the conductance of a quantum wire embedding a one-dimensional magnetic superlattice. They found that the number of resonant splittings in the first conduction plateau has no simple direct correspondence to the number of unit cells of the superlattice. In this paper, we calculate the transport properties of a quantum wire embedding a finite-length saw-tooth superlattice under magnetic modulation using the recur-

*Project supported by National Major Project of China (Grant No 1999-0645-4500), and Scientific Research Fund of Hunan Provincial Education Department, China (Grant No 02C572).
†Corresponding author: xhyan@xtu.edu.cn
‡E-mail: chenyp@xtu.edu.cn

sive Green function (RGF) method. In order to study electron transport of quantum systems, several numerical methods such as mode-matching method,[3] RGF method,[1,10−14] and the transfer matrix approach [15] have been extensively applied. In these methods, the RGF method uses a lattice model, i.e. a discretization of space. This is convenient in the presence of a magnetic field which is incorporated simply in the form of a Peierls phase factor of the transfer integral.[16] This paper is organized as follows. In Section 2, the model and method are described briefly. In Section 3, we discuss the effect of geometry of the structure and the strength of magnetic field on electron transport through a quantum wire embedding a single saw-tooth quantum dot (QD). Based on the quantum wire embedding a single QD, transmission properties of a quantum wire embedding a finite-length superlattice which comprises several saw-tooth QDs under a periodic magnetic field are studied. The influence of QD number and field strength on minibands and resonant splitting of the structure is discussed. A brief summary is concluded in Section 4.

2. Model and method

Consider a multi-section quantum wire which consists of two semi-infinite quantum wires embedding a quantum potential structure (Fig.1). In Fig.1(a), a saw-tooth cavity (III) connected with narrow constrictions (II and IV) is embedded between two semi-infinite quantum wires (I and V). The cavity is usually referred to as a QD.[17] Cascading several QDs to substitute the single QD, we can obtain a structure of a quantum wire embedding a finite-length superlattice (see Fig.1(b)). In terms of the RGF scheme, one divides the system into a set of effective square lattices with lattice constant a that is much smaller than all the other length scales of the problem (see Fig.1(a)). Hard wall boundaries are simply simulated by the absence of sites. To describe the electronic properties of the effective discretized system of square lattice, one can define the tight-binding Hamiltonian as [10]

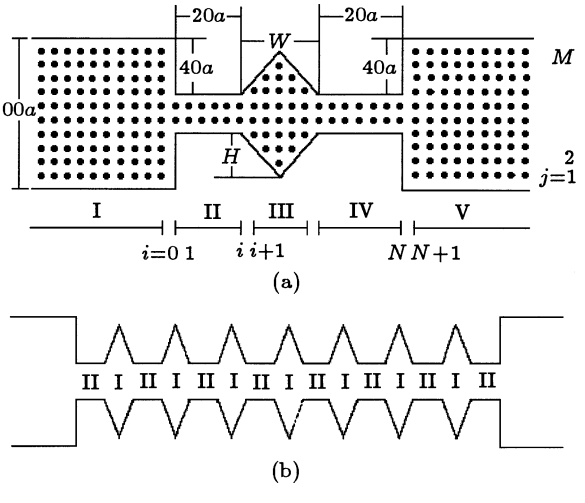


Fig.1. (a) A quantum wire embedding a saw-tooth QD. (b) A quantum wire embedding a finite-length superlattice which consists of seven saw-tooth QDs.

$$\begin{aligned} H = & \sum_{i,j} \varepsilon_{i,j} |i,j\rangle \langle i,j| \\ & + \sum_{i,j} V_1(|i,j\rangle \langle i,j+1| + \text{H.c.}) \\ & + \sum_{i,j} V_2(|i+1,j\rangle \langle i,j| + \text{H.c.}), \end{aligned} \tag{1}$$

where H.c. denotes the Hermitian conjugate, $\varepsilon_{i,j}$ is the site energy at (i,j) site, and V_1 and V_2 are transverse and longitudinal hopping matrix elements between nearest neighbouring sites respectively. We divide the Hamiltonian into two parts in the column cell

$$H = \sum_i H_i + \sum_i (H_{i,i+1} + H_{i+1,i}), \tag{2}$$

where H_i is the Hamiltonian of the ith isolated column cell, $H_{i,i+1}$ and $H_{i+1,i}$ are intercell Hamiltonian between the ith column cell and the $(i+1)$th column cell with

$$H_{i+1,i} = \widetilde{H}^*_{i,i+1} \,. \tag{3}$$

So the first two terms of Eq.(1) correspond to the first term of Eq.(2) and the last term of Eq.(1) corresponds to the second term of Eq.(2). Generally, $\varepsilon_{i,j} = -4V$ and $V_1 = V_2 = V = -\hbar^2/2m^*a^2$ (m^* is the effective mass of electron, and one sets $m^* = 0.067m_0$) in the absence of magnetic modulation.[11] When applying a magnetic field B which is normal to the plane of paper to region III of Fig.1(a), $V_1 = V$ and V_2 in region III should be written as [11]

$$V_2 = V \exp(2\pi i B' j), \tag{4}$$

with $B' = \Phi/\Phi_0$, $\Phi = Ba^2$, $\Phi_0 = h/e$, in terms of the Peierls phase factor of transfer integral.[16]

In the RGF method, one can use a recursive scheme to evaluate the systematic Green function associated with the Hamiltonian given by Eq.(2). In terms of the definition of Green function $G = (E - H)^{-1}$, we construct the diagonal and off-diagonal Green function by

$$\begin{aligned} \langle i| G^i |i\rangle &= \langle i| (E - H^i) |i\rangle^{-1}, \\ \langle i| G^i |0\rangle &= \langle i| (E - H^i) |0\rangle^{-1}, \end{aligned} \tag{5}$$

where E is the energy of electron, and H^i is the total Hamiltonian for the strip comprising column cells from 0th to ith. In particular, $\langle 0|\, G^0\, |0\rangle$ of the 0th column cell (the last column cell of the left semi-infinite quantum wire) and $\langle N+1|\, G^{N+1}\, |N+1\rangle$ of $(N+1)$th column cell (the first column cell of the right semi-infinite quantum wire) represent Green functions of the left and right semi-infinite quantum wires respectively. So $\langle N+1|\, G\, |0\rangle$ represents the systematic Green function which couples those from the 0th to the $(N+1)$th column cell (see bottom panel of Fig.1(a)). According to the Dyson equation $G = G^0 + G^0 \hat{V} G$, a set of recursive formulae can be obtained:[11]

$$\begin{aligned} &\langle i+1|\, G^{i+1}\, |i+1\rangle^{-1} \\ =&E - H_{i+1} - H_{i+1,i}\, \langle i|\, G^i\, |i\rangle\, H_{i,i+1}, \qquad (6) \\ &\langle i+1|\, G^{i+1}\, |0\rangle \\ =&\langle i+1|\, G^{i+1}\, |i+1\rangle\, H_{i+1,i}\, \langle i|\, G^i\, |0\rangle\,. \qquad (7) \end{aligned}$$

We start recursion from $\langle 0|\, G^0\, |0\rangle$. In Eq.(6), the following sequences of Green functions: $\langle 0|\, G^0\, |0\rangle \to \langle 1|\, G^1\, |1\rangle \to \cdots \to \langle N|\, G^N\, |N\rangle$ can be generated. Substituting these Green functions into Eq.(7), we can obtain $\langle 1|\, G^1\, |0\rangle \to \langle 2|\, G^2\, |0\rangle \to \cdots \to \langle N|\, G^N\, |0\rangle$ in turn. In the final recursion step we attach the right semi-infinite quantum wire, and then obtain the Green function $\langle N+1|\, G\, |0\rangle$.

Utilizing the Green function $\langle N+1|\, G\, |0\rangle$, the transmission amplitude can be calculated. Suppose semi-infinite quantum wires consist of M lattice sites, namely M channels in the transverse direction (see Fig.1(a)), the transmission coefficient $t_{\alpha\beta}$ for the incident channel β with velocity ν_β and out-going channel α with velocity ν_α is [11]

$$\begin{aligned} t_{\alpha\beta} =& \left[\frac{\nu_\alpha}{\nu_\beta}\right]^{\frac{1}{2}} \{V\, \Psi^{-1}(+) \langle N+1|G|0\rangle \\ &\times P[F^{-1}(+) - F^{-1}(-)]\, \Psi(+)\}_{\alpha\beta}, \qquad (8) \end{aligned}$$

where $F(\pm) = \Psi(\pm) \Lambda(\pm) \Psi^{-1}(\pm)$, and P is a $M \times M$ matrix consisting of phase factors caused by magnetic field B_1 in semi-infinite quantum wires

$$P_{l,l'} = \exp(2\pi i e B_1 a^2 l/h)\delta_{l,l'} \quad (l, l' = 1, \cdots, M). \qquad (9)$$

Wavefunction matrices

$$\Psi(\pm) = (\, \Psi_1^{\pm} \quad \Psi_2^{\pm} \cdots \Psi_M^{\pm}) \qquad (10)$$

and

$$\Lambda(\pm) = \begin{bmatrix} \lambda_1^{\pm} & & \\ & \ddots & \\ & & \lambda_M^{\pm} \end{bmatrix} \qquad (11)$$

satisfy the eigen-equation

$$\lambda \begin{pmatrix} \Psi_i \\ \Psi_{i-1} \end{pmatrix} = \begin{bmatrix} V^{-1}(E - H_0) & -P^2 \\ 1 & 0 \end{bmatrix} \begin{pmatrix} \Psi_i \\ \Psi_{i-1} \end{pmatrix}, \qquad (12)$$

where H_0 is the Hamiltonian of a column cell in semi-infinite quantum wires and it is a $M \times M$ matrix given by

$$H_0 = \begin{bmatrix} -4V & V & \cdots & 0 \\ V & -4V & \cdots & 0 \\ \cdots & \cdots & \ddots & \cdots \\ 0 & 0 & \cdots & -4V \end{bmatrix}. \qquad (13)$$

Here $\Psi_1^+,\ \Psi_2^+, \ldots, \Psi_M^+$ are wavevectors of the right-going solutions corresponding to $\lambda_1^+, \lambda_2^+, \ldots, \lambda_M^+$; and $\Psi_1^-,\ \Psi_2^-, \ldots,\ \Psi_M^-$ are wavevectors of the left-going solutions corresponding to $\lambda_1^-,\ \lambda_2^-, \ldots,\ \lambda_M^-$. The Green functions of left and right semi-infinite quantum wires can be obtained, respectively, by [13]

$$\langle 0|G^0|0\rangle = V^{-1} F^{-1}(-) P, \qquad (14)$$

$$\langle N+1|G^{N+1}|N+1\rangle = V^{-1} F(+) P^*. \qquad (15)$$

If the magnetic field is absent in the two semi-infinite quantum wires, the formulation (8) can be simplified as

$$\begin{aligned} t_{\alpha\beta} =& \left[\frac{\nu_\alpha}{\nu_\beta}\right]^{\frac{1}{2}} \{V\, \Psi^{-1}(+) \langle N+1|G|0\rangle \\ &\times [F^{-1}(+) - F^{-1}(-)]\, \Psi(+)\}_{\alpha\beta}. \qquad (16) \end{aligned}$$

Then

$$T = \sum_{\beta=1}^{M} \sum_{\alpha=1}^{M} |t_{\alpha\beta}|^2.$$

According to the Landauer formula, the conductance of the two-terminal system is

$$G = \frac{2e^2}{h} T. \qquad (17)$$

3. Numerical results and discussion

We first discuss the effect of geometric structure on the transmission coefficient for a quantum wire embedding a single saw-tooth QD (Fig.1(a)). In Fig.2, we show the correlation between transport properties and the size of a single QD in the absence of magnetic field. It is found that the transmission oscillations T

are closely related to the size of QD. As the longitudinal size W of saw-tooth stubs is constant (Fig.2(a)), a prominent peak is observed below the first subband threshold energy of constrictions ($E \approx 0.075$ in units of the hopping matrix element $|V| = \hbar^2/2m^*a^2$). The peak is due to the resonant tunnelling through the quasibound state of QD. As the energy of electrons is relatively low ($E < 0.158$), electronic transport is independent of transverse size H of saw-tooth stubs except that the quasibound-peaks have a small shift. For $E > 0.158$, the sharpness of saw-tooth QD induces more transmission 'zeros' [18] (not shown here), i.e. more transmission oscillations. It can be generally interpreted by the fact that electrons with a relatively low energy cannot penetrate the stubs due to the higher zero-point energy marking the threshold for propagation in the stubs.[1] So the transport of low-energy electrons is insensitive to the variation of lateral width. However, higher-energy electrons can travel along the stubs with different wavelengths,[19] and thus more channels resonant with the incident energies in the stubs make the transport more complex. Since H is a constant (Fig.2(b)), the thickness of QD may affect the transport of both low- and high-energy electrons. With the increase of W, the position of quasibound-peak shifts distinctly to low energy side. This indicates that the energy of quasibound-state decreases with the increase of transverse size of QD. High-energy electrons which can penetrate the stubs exhibit complex oscillation like the case in Fig.2(a). In addition, a comparison between the two dotted lines in Figs.2(a) and 2(b) shows that the two QDs with the same stub area have nearly the same transmission zero ($E \approx 0.243$). This means that the transmission zeros are associated with the interplay between stubs and uniform quantum wire.

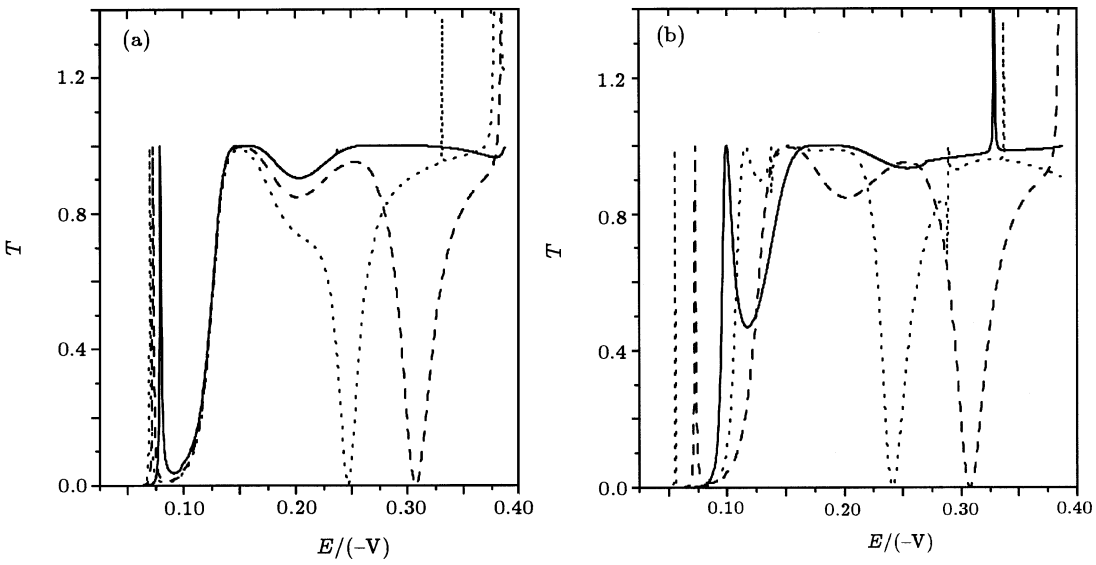


Fig.2. Transmission coefficient T for a quantum wire embedding a saw-tooth QD. (a) $W = 20a$ is constant and the values of H are chosen to be $10a$, $20a$, $30a$ for solid, dashed, dotted lines respectively. (b) $H = 20a$ is constant and the values of W are chosen to be $10a$, $20a$, $30a$ for solid, dashed, dotted lines respectively. Electron energy E is in units of hopping energy $-V$.

In Fig.3, we calculate the transmission coefficient T for the structure in Fig.1(a) when the QD is subjected to a perpendicular magnetic field. Figure 3(a) shows a weak magnetic modulation to the transport of electrons. It is seen that the quasibound peak shifts towards the high-energy region with the increase of field strength. This is due to the field modulation increasing the quasibound-state energy. Transmission amplitude in high-energy region exhibits more oscillations under weak magnetic modulation. For example, in the energy range $0.0978 < E < 0.305$, the resonant domain at zero field (solid line in Fig.3(a)) splits into two domains at $B = 0.07$ (in units of $-m^*V/\hbar e$) (dashed line in Fig.3(a)). This suggests that weak magnetic modulation makes the quantum interference effect in QD more pronounced. As magnetic modulation is strengthened, the high-lying modes are depleted [5] and mode-mixing in QD is reduced. Therefore, drastic oscillations caused by mode mixing are suppressed and high-energy electrons exhibit a big

transmission amplitude ($T \sim 1$), as shown in Fig.3(b). Meanwhile, the quasibound peak shifts to the high-energy side and vanishes gradually. As the modulation strength is very large, as expressed by the dotted line in Fig.3(b), the electron transport in the QD is dominated by edge states. Then an effective loop of edge states (see the inset in Fig.3(b)) is formed, leading to the loss of the electron transmission through the QD. So the transmission amplitude recovers a quantization plateau: that is, electrons with lower energy than the threshold of the first 'bulk' Landau level ($E \approx 0.176$) are mostly blocked, while high-energy electrons can pass through the QD nearly unscattered.

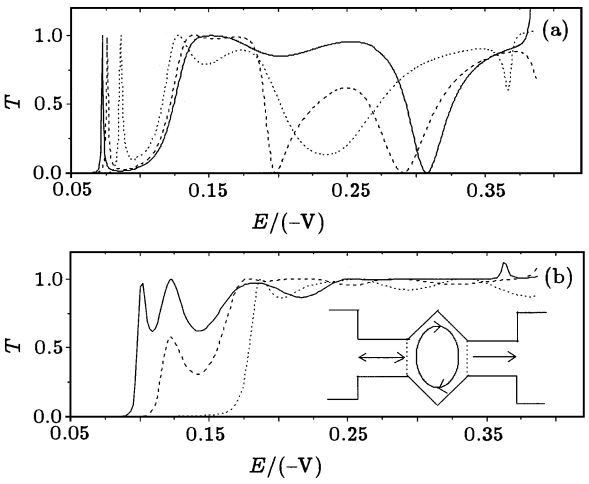


Fig.3. Transmission coefficient T versus energy E of incident electron for the structure in Fig.1(a), on applying different magnetic field B to the saw-tooth QD with $W = 20a$, $H = 20a$. (a) The values of B for the solid, dashed, dotted lines are 0, 0.07, 0.14, respectively. (b) The values of B for the solid, dashed, dotted lines are 0.21, 0.28, 0.35 respectively. B is in units of $-m^*V/\hbar e$.

When one strings several QDs into a sequence and then inserts it into a quantum wire, it becomes a structure of a quantum wire embedding a finite periodic superlattice (Fig.1(b)). To reveal the correlation among the resonant splittings, the formation of minibands and the periodic number of a finite superlattice, we show the transport properties of the structure consisting of n QDs without field modulation in Fig.4. In the low-energy region ($E < 0.0978$), the resonant peak splitting of transmission amplitude is n-fold, while the resonant peak splitting in other energy regions is $(n-1)$-fold. It is known that resonant peak splitting is closely associated with the quantum discrete states residing in the superlattice. These discrete states originate from the coupling of the quasizero-dimensional states formed between the constrictions. So the number of resonant peak splittings should be equal to the number of QDs, i.e. the resonant peak splitting should be n-fold like the electric superlattice and magnetic superlattice [20−22] in two-dimensional electron gas (2DES). The vacancy of resonant peak splitting at the high-energy region may be due to the presence of multiple modes and the mode-mixing effect.[8] It should also be noted that, for $0.0978 < E < 0.305$, the shallow valley of the resonant domain gradually drops and subsequently turns into a minigap with increasing n (see Figs.4(a) through 4(d)). This leads to the resonant domain in Fig.4(a) splitting up into two domains (minibands). Transmission zero ($E \approx 0.305$) extends to form a minigap followed by a resonant domain emerging in the middle of the minigap. The formation of minibands and minigaps is due to the period of finite-length superlattice being much bigger than the lattice constant. So energy bands may split into minibands of the finite superlattice. In spite of fewer periods here, the position of minibands and minigaps agrees well with that in the multiple even infinite periods case. As the magnetic field is applied to QD(s) of finite-length superlattice, as shown in Fig.5, the formation process of minibands and minigaps is similar to that in Fig.4. By comparing Fig.5 with Fig.4, one finds that the modulation may shift the positions of miniband and minigap of the superlattice. Accordingly, weak magnetic modulation to QD(s) leads to the increase of the number of resonant domains. Another character induced by magnetic modulation deserves special attention—resonant splitting in the second resonant domain in Fig.5 is n-fold but not $(n-1)$-fold like that in Fig.4. This may be due to the elimination of degeneration in the energy range by magnetic modulation. In addition, Figs.4 and 5 show that the width of minibands is narrowed and the minigaps followed by minibands are well formed with the increase of the period number of superlattice. Incident electrons with their energies lying in the minibands can pass through the finite-length superlattice, while the transport of electrons is blocked if the energy of incident electrons falls in the minigap region. It is indicated that these kinds of structures can serve as energy filter.[23] This may provide a way to tailor transmission spectrum to match demands through altering the sizes of saw-tooth QD and field strength.

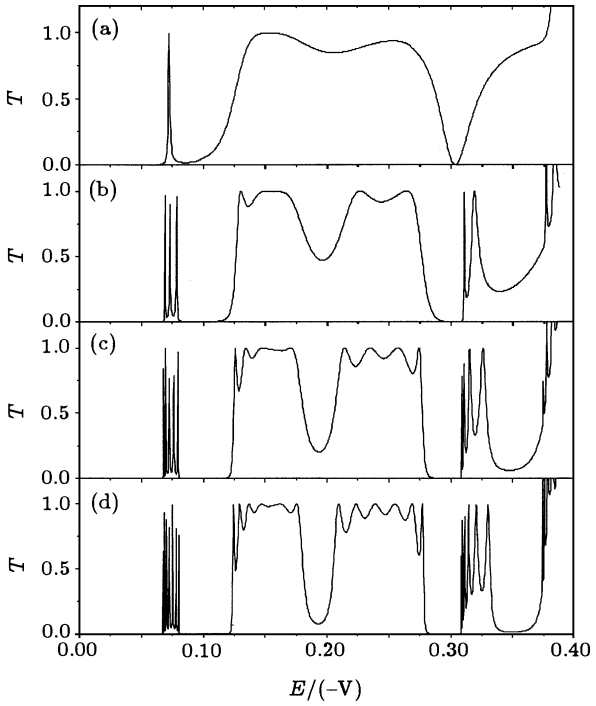


Fig.4. Transmission coefficient T versus incident-electron energy E for a finite-length superlattice comprising n saw-tooth QD(s) with $H = 20a$, $W = 20a$, embedded in a quantum wire at zero field. The size of semi-infinite quantum wires and constrictions is same as in Fig.1(a). (a) $n = 1$. (b) $n = 3$. (c) $n = 5$. (d) $n = 7$.

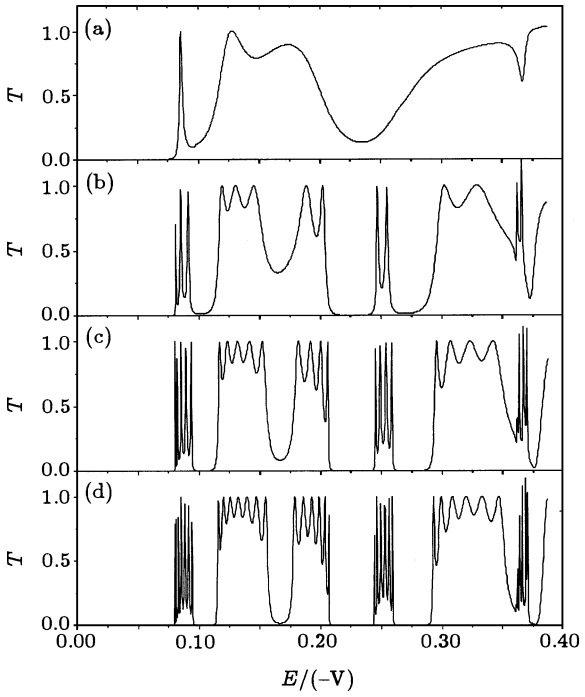


Fig.5. Transmission coefficient T versus incident-electron energy E for a finite-length superlattice comprising n saw-tooth QD(s) with $H = 20a$, $W = 20a$, embedded in a quantum wire as QD(s) is (are) subjected to a magnetic field B=0.14. The size of semi-infinite quantum wires and constrictions is same as in Fig.1(a). (a) $n = 1$. (b) $n = 3$. (c) $n = 5$. (d) $n = 7$.

To examine the modulation of magnetic field in QD(s), we plot, in Figs.6 and 7, the conductance versus incident-electron energy in a wide range for the structures described in Figs.1(a) and 1(b) respectively. Conductance spectrum in Fig.6(a) shows a series of resonant peaks, due to the effect of quantum interference and backscattering caused by abrupt change of quantum wire width. In Figs.6(b) and 6(c), the peaks are substantially smoothed out and quantization plateau is gradually recovered by the application of a magnetic field to the QD. This originates from the formation of edge states. Because of the coupling between the quasizero-dimensional states, energy bands of a quantum wire embedding a single QD may split into minibands and minigaps in the superlattice consisting of multiple QDs. Furthermore, the multi-period of superlattice increases the disorder and then enhances the backscattering. So the resonant peaks of conductance in Fig.7(a) become sharper and much denser than those in Fig.6(a). Conductance exhibits a behaviour of fluctuation. As a magnetic field is applied to region I of Fig.1(b), i.e. a periodic magnetic field in the superlattice, the magnetic modulation strengthens the localization, and the additional effective potential induced by the magnetic field increases backscattering. So the conductance falls rapidly with the increase of field strength, as shown in Figs.7(b) and 7(c).

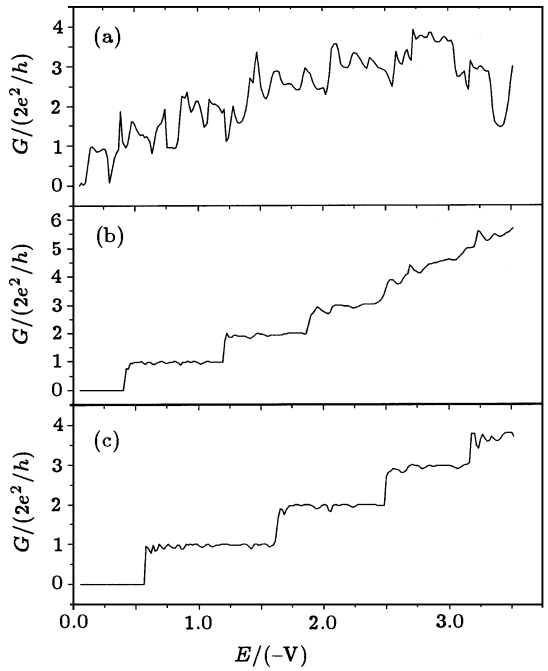


Fig.6. Conductance G (in units of $2e^2/h$) versus incident-electron energy E for the structure in Fig.1(a), on applying different magnetic fields B to saw-tooth QD with $H = 20a$, $W = 20a$. (a) B=0. (b) B=0.88. (c) B=1.23.

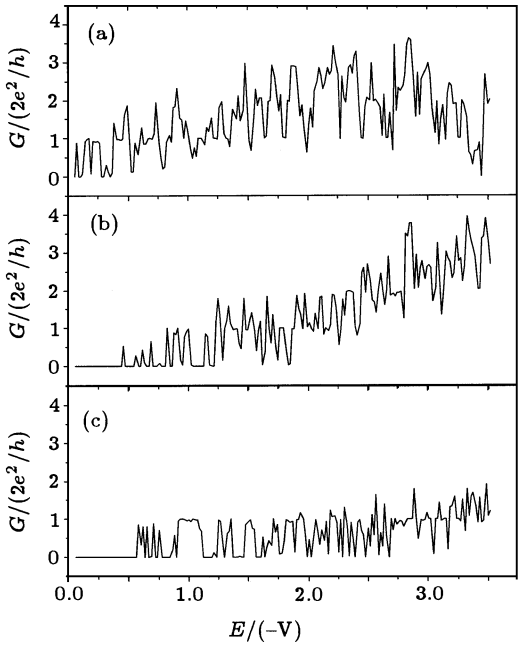


Fig.7. Conductance G (in units of $2e^2/h$) versus incident-electron energy E for the structure in Fig.1(b), on applying different magnetic fields B to region I. (a) B=0. (b) B=0.88. (c) B=1.23. The size of semi-infinite quantum wires and constrictions in Fig.1(b) is the same as in Fig.1(a) with $W = 20a$, $H = 20a$.

4. Conclusions

We have studied electron transport across a quantum wire embedding a finite-length saw-tooth superlattice using the RGF method. For a quantum wire embedding a single saw-tooth QD, the transport of low-energy electron is independent of the QD's transverse width except that the quasibound state has a small shift. The transmission zeros are closely associated with the interplay between stubs and the uniform quantum wire. When the QD is subjected to a weak magnetic field, quantum interference in the QD becomes more pronounced. The increase of field modulation may weaken the interference. Under a large field, quantization plateau of transmission coefficient is recovered. When a quantum wire embeds a finite-length saw-tooth superlattice consisting of n QDs, it is found that the resonant peak splitting in resonant domains is $(n-1)$-fold except that the quasibound peak splitting is n-fold at zero field. Applying a periodic weak magnetic field to the superlattice, the number of splittings of the second resonant domain increases by one, and the total resonant domains also increase. The effect of these kinds of structures are similar to an energy filter. One can tailor transmission spectrum to match the demands for application through altering the sizes of saw-tooth QD and field strength. In a wide energy range, resonant peaks in conductance become sharper and denser with increasing period number of the superlattice. When we apply a stronger magnetic modulation to QDs of the superlattice, localization and backscattering may reduce the conductance rapidly.

References

[1] Sols Fernando, Macucci M, Ravaioli U and Hess Karl 1989 *J. Appl. Phys.* **66** 3892

[2] Wang C K and Jiang Z T 2000 *Acta Phys. Sin.* **49** 1574 (in Chinese)

[3] Weisshaar Andreas, Lary Jenifer, Goodnick Stephen M and Tripathi Vijai K 1991 *J. Appl. Phys.* **70** 355

[4] Ando T 1990 *Phys. Rev.* B **42** 5626

[5] Takagaki Y and Ploog K 1995 *Phys. Rev.* B **51** 7017

[6] Kouwenhoven L P, Hekking F W J, Wees B J van, Harmans C J P M, Timmering C E and Foxon C T 1990 *Phys. Rev. Lett.* **65** 361

[7] Xu H Q 1995 *Phys. Rev.* B **52** 5803

[8] Gu B Y, Zhang Y and Wang X H 2000 *J. Appl. Phys.* **88** 300

[9] Ji Z L and Sprung D W L 1996 *Phys. Rev.* B **54** 8044

[10] Kawamura T and Leburton J P 1993 *Phys. Rev.* B **48** 8857

[11] Ando T 1991 *Phys. Rev.* B **44** 8017

[12] Sanvito S, Lambert C J, Jefferson J H and Bratkovsky A M 1999 *Phys. Rev.* B **59** 11936

[13] MacKinnon A 1985 *Z. Phys.* B **59** 385

[14] Macucci M, Galick A and Ravaioli U 1995 *Phys. Rev.* B **52** 5210

[15] Wang R Z and Yan X H 2000 *Chin. Phys. Lett.* **8** 589

[16] Peierls R 1933 *Z. Phys.* **80** 763

[17] Silvan U, Imry Y and Hartzstein C 1989 *Phys. Rev.* B **39** 1242

[18] Porod Wolfgang, Shao Z A and Lent Craig S 1992 *Appl. Phys. Lett.* **61** 1350

[19] Xia J B and Sheng W D 1996 *J. Appl. Phys.* **79** 7780

[20] Zeng Z Y, Zhang L D, Yan X H and You J Q 1999 *Phys. Rev.* B **60** 1515

[21] Guo Y and Gu B L 1999 *Acta Phys. Sin.* **48** 1733 (in Chinese)

[22] Guo Y, Gu B L, Li Z Q, Sun Q and Kawazoe Y 1998 *Eur. Phys. J.* B **3** 257

[23] Yang Q K and Li A Z 2000 *J. Appl. Phys.* **87** 1963